

Mechanistic Aspects of Proton Chain Transfer: A Computational Study for the Green Fluorescent Protein Chromophore

Sufan Wang and Sean C. Smith*

Centre for Computational Molecular Science, Chemistry Building #68, The University of Queensland, Brisbane, Queensland 4072, Australia

Received: November 30, 2005; In Final Form: January 16, 2006

We explore several models for the ground-state proton chain transfer pathway between the green fluorescent protein chromophore and its surrounding protein matrix, with a view to elucidating mechanistic aspects of this process. We have computed quantum chemically the minimum energy pathways (MEPs) in the ground electronic state for one-, two-, and three-proton models of the chain transfer. There are no stable intermediates for our models, indicating that the proton chain transfer is likely to be a single, concerted kinetic step. However, despite the concerted nature of the overall energy profile, a more detailed analysis of the MEPs reveals clear evidence of sequential movement of protons in the chain. The ground-state proton chain transfer does not appear to be driven by the movement of the phenolic proton off the chromophore onto the neutral water bridge. Rather, this proton is the last of the three protons in the chain to move. We find that the first proton movement is from the bridging Ser205 moiety to the accepting Glu222 group. This is followed by the second proton moving from the bridging water to the Ser205—for our model this is where the barrier occurs. The phenolic proton on the chromophore is hence the last in the chain to move, transferring to a bridging “water” that already has substantial negative charge.

1. Introduction

The green fluorescent protein (GFP) has been the subject of intense interest because of its unique photophysical properties, which are being elucidated in progressively greater detail by a great variety of spectroscopic techniques.^{1–5} These properties are now exploited ubiquitously for imaging studies of protein folding, gene expression, and protein trafficking and cell development.^{1,6–8} A detailed molecular understanding of the biophysics of the GFP and related fluorescent proteins (FPs) is not a prerequisite for their practical utilization in imaging applications. However, to realize the enormous range of possible applications for FPs, there is a demand for new proteins that are both more brightly fluorescent and whose absorption and emission maxima span a wider spectral range. This developmental work demands a much more profound understanding of the photophysical properties of the chromophore as well as the subtleties of its interactions with the surrounding protein matrix.⁹ First-principles theoretical studies as well as spectroscopic experiments will play an important role in this regard.

The GFP is widely regarded to exist under ambient conditions in two forms that are related by deprotonation of the *p*-hydroxybenzylideneimidazolidinone chromophore through a proton shuttle equilibrium that favors the neutral form *in vivo*. Upon absorption of light, the neutral form is photoconverted into the anionic form by excited-state proton transfer.^{2,10} In this context, “neutral” and “anionic” refer to the charge state of the chromophore. X-ray studies have provided a picture in which hydrogen-bonding networks involving the chromophore, a finite number of localized water molecules, and neighboring amino acid residues are central to the existence of different forms of the chromophore and to the occurrence of excited-state proton

transfer (ESPT).¹¹ The proposed mechanism for the photoisomerization of wild-type GFP involves conversion of the neutral form of the chromophore (A) to the anionic form (B) through an intermediate state (I). In going from the neutral species (A) to the charged species (B), the Tyr66 phenolic proton is shuttled through a hydrogen-bonding network to the carboxylate oxygen of Glu222. The change from A to I is solely a protonation change involving the movement of three protons, while the transition from I to B is a conformational change occurring mostly at Thr203.^{2,11–13}

The mechanism summarized above for the fluorescence in wild-type GFP has been inferred from accumulated experimental evidence, and there exist also a number of modeling studies that support various aspects of this mechanism.¹⁴ Zimmer and co-workers have used molecular mechanics to explore issues relating to the structural relaxation from the I state to the B state via a rotation of the Thr203 residue and also internal torsion of the chromophore, which may lead to radiationless conversion to the ground state.^{12,13,15} Langhoff and co-workers have carried out exploratory *ab initio* calculations to investigate the mechanism of internal conversion via torsional motions within the chromophore.¹⁶ Several other studies have subsequently explored this issue in further detail.^{17–19} Vendrell et al.²⁰ have recently raised the possibility that the proton-transfer coordinate from the chromophore to a neighboring water molecule may mediate crossing from the photoexcited $^1\pi\pi^*$ state to a $^1\pi\sigma^*$ charge-transfer state, representing another possible radiationless relaxation pathway that is analogous to the case of phenols.²¹ Our mechanistic conclusions in this work have some bearing on their conclusions, and we return to this in our discussion below. Laino et al.²² have proposed a scaling law for the dependence of the optical absorption wavelength of the chromophore on the surrounding residues, based on density functional theory (DFT) calculations for a training set of cluster

* Author to whom correspondence should be addressed. E-mail: s.smith@uq.edu.au.

models involving different surrounding moieties. The key parameter that reveals the linear correlation relates to the degree of single/double bond alternation in the chromophore, a ground-state geometrical parameter that can be calculated via DFT without recourse to sophisticated methods that are required for convergence of the optically bright excited state. Lill and Helms²³ have implemented molecular dynamics calculations together with a stochastic jump mechanism for incorporating the quantum proton-transfer rates in an approximate manner. Also worthy of note is the development of a CHARMM force field for representation of the chromophore in GFP by Thiel and co-workers, which will help in the implementation of more reliable molecular dynamical studies.²⁴ Meech²⁵ has stressed that the best way to represent the complex and delicate interactions between the chromophore and the protein matrix is through quantum chemical calculations, an agenda that clearly presents major challenges for current quantum chemical codes.

In the present work, we focus on the complex proton-transfer process that links the neutral "A" state and the anionic "I" state (prior to any subsequent structural rearrangements occurring on a longer time scale) of the GFP chromophore in its ground electronic state. Although proton chain transfer reactions happen in a number of important biological systems other than the GFP, detailed computational studies elaborating the nature of the proton-transfer pathways are still few in number. In addition to the complexities of locating saddle points and pathways, achieving a level of convergence in the quantum chemical calculations that will enable quantitative conclusions to be drawn remains a highly challenging proposition. An issue that has received some attention in recent literature is whether the mechanism for such chain transfer reactions should be regarded as stepwise or concerted.^{26–32} If the proton chain transfer is stepwise, then the protons involved will shuttle along the hydrogen-bonded chain in a sequential manner via a series of kinetically stable intermediates. Contrastingly, for the concerted mechanism all of the relevant protons would undergo substantive motion simultaneously.

A stepwise mechanism, if operative, may provide some simplifications from a first-principles modeling perspective. One might be able to compute the barrier for each proton hop independently with a localized quantum chemical system that includes only the instantaneous donor and acceptor groups explicitly. This type of approach has been adopted in an approximate fashion by Helms and co-workers^{28–30} in their studies of GFP. A concerted mechanism, however, is intrinsically more demanding since it requires a much more extended system to be explicitly incorporated into the quantum chemical calculation of the potential barrier. Zhang et al.³³ have recently published an excellent illustration of this type of calculation in a model for the GFP chromophore and its proton chain transfer pathway. Cui and Karplus have reported a similar study for a model of the carbonic anhydrase enzyme.³¹

We examine here several models for the proton-transfer pathway that links the neutral and anionic forms of the GFP on the electronic ground-state potential energy surface. We compute intrinsic reaction pathways for these models, examination of which leads to significant conclusions concerning the mechanistic question highlighted above. In a manner similar to Zhang et al.,³³ we have adopted the strategy of formulating model systems that contain the GFP chromophore and certain small molecules that mimic nearby residues thought to be key players in the proton-transfer pathway. Quantum chemical calculations are performed for these systems to explore the nature of the reaction pathway that describes the proton chain transfer. Our

systems are cluster models set up in a vacuum. This allows us to gain preliminary insight into the intrinsic properties of the chromophore and the immediate proton-transfer pathway, in the absence of subtle and complex interactions with the other surrounding residues of the enveloping protein matrix. Full protein (QM/MM) studies may then reveal the way in which these "environmental" interactions modify the intrinsic picture arising from the present study. However, the challenges of capturing these subtle interactions reliably in a QM/MM calculation should not be underestimated.

In section 2, we describe the cluster models that are studied in this work. Section 3 provides results from some benchmarking of electronic structure methods on the two-proton chain transfer model, which leads us to adopt the B3LYP/6-31+g** methodology for the subsequent calculations. Section 4 presents the results obtained for energetics, structures, and reaction pathways as well as mechanistic analysis. Discussion of the results and some consideration of their contextual significance is given in section 5, followed by conclusions in section 6.

2. The Models

From earlier studies,^{34–38} the molecule, 4'-hydroxybenzylidene-2,3-dimethyl-imidazolinone (HBDI) is chosen as the model for the GFP chromophore. This model is generated by cutting the linkages from the chromophore moiety to the protein matrix and saturating with two methyl groups. The proton-transfer pathway in GFP is understood to involve movement of the proton on the chromophore to a bridging water molecule, whose position is localized through hydrogen-bonding interactions. The water molecule passes a proton to the terminal alcohol group on the neighboring Ser205 residue. This terminal alcohol group passes a proton to the terminal carboxylate group on the Glu222 residue. The carboxylate group, being negatively charged under ambient conditions, then becomes a neutral carboxylic acid and constitutes the end of the immediate proton-transfer pathway.^{2,11–13} In light of this, we incorporate the following moieties in our models for the proton chain transfer: (a) HBDI as donor, representing the GFP chromophore, (b) H₂O as the first bridging molecule, (c) CH₃OH as the second bridging molecule, representing the terminal group on Ser205, and (d) HCO₂[−] as the acceptor, representing the deprotonated terminal group on Glu222.

We examine three models of differing complexity. A one-proton-transfer model is constituted by the HBDI donor and HCO₂[−] acceptor alone, without any bridging species. A two-proton chain transfer model is constituted by the HBDI donor, H₂O bridge, and HCO₂[−] acceptor. Finally, a three-proton chain transfer model is constituted by the HBDI donor, H₂O bridge, CH₃OH bridge, and HCO₂[−] acceptor. The neutral stationary configurations of each of these models are shown in Figure 1, optimized at B3LYP/6-31+g** (recall that "neutral" here refers to the protonation state of the chromophore). We note in passing that many stationary points exist for these clusters, most of which are not relevant for our current purposes.

3. Characterization of Methods

As the two-proton model described above is the simplest example of a chain transfer process, we base our discussion of methods around this model. Figure 2 shows a series of two-dimensional (2-D) relaxed potential energy surfaces calculated at different levels of theory and basis sets. The method of construction of these surfaces has been discussed in detail in our earlier work.³⁹ In brief, these are essentially two-dimensional analogues of the more common 1-D relaxed potential scans

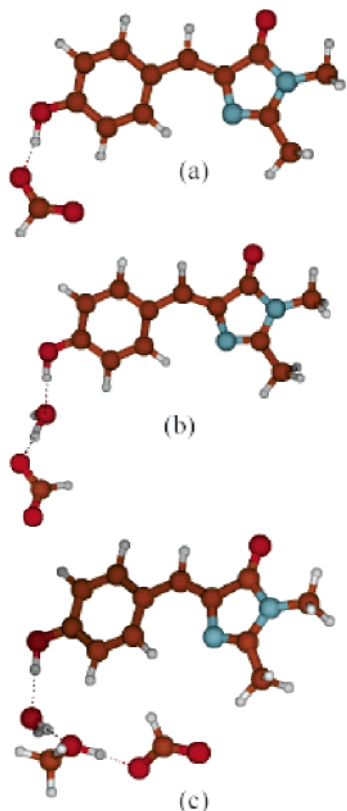


Figure 1. Stationary starting geometries for the three proton-transfer models, optimized at B3LYP/6-31+g**: (a) single-proton model with donor HBDI and acceptor HCO_2^- ; (b) two-proton model including bridging water; and (c) three-proton model including bridging water and bridging methanol.

based on the leading coordinate approach. In the earlier work, it was demonstrated that apparently plausible guesses at the reaction coordinate (e.g., the donor–H1 bond length) can lead to 1-D potential scans with apparent barriers that are misleadingly small and in fact spurious; this fact was easily picked up by tracing the geometries of the 1-D scan on the 2-D surface. For the present purposes, the 2-D plots shown here provide some additional topological information about the PES (beyond what is furnished by a 1-D potential energy profile) that is helpful in exploring the behavior of different levels of theory and basis sets as well as revealing something of the geometric character of the minimum energy pathways (MEPs).

Figure 2a shows the relaxed surface calculated at HF/6-31g*. All degrees of freedom for the two-dimensional relaxed potential energy surfaces are relaxed except the hydrogen bond lengths shown on the axes and the internal geometry of the HBDI chromophore, which is frozen at that of the neutral complex. Also shown as a dashed line is an approximate MEP, estimated directly from the surface. The full MEP (without artificial geometry constraints) was not converged with this basis set. In Figure 2b, single-point energy calculations are carried out over the grid of 19×20 points at the same HF/6-31g* optimized geometries but with the basis set now increased to 6-31+g**. While the overall features of the surface are similar, the larger basis set is better behaved with respect to finding the true MEP, which is now converged and represented on the diagram by the dotted line. Figure 2c shows the surface obtained using B3LYP/6-31+g**//HF/6-31g*. Density functional theory predicts the neutral cluster to be more weakly bound, with the barrier for proton transfer being almost negligible. Finally, Figure 2d shows the MP2/6-31+g**//HF/6-31g* surface. Again,

the neutral cluster is more weakly bound in comparison to the HF predictions, and the barrier to proton transfer is somewhat higher than the DFT calculation but still significantly smaller than the HF predictions. The energetics implicit in Figure 2 are summarized numerically in Table 1.

On the basis of the results of Figure 2 and Table 1, we have adopted the B3LYP/6-31+g** method in this work for more extended exploration of the one-, two-, and three-proton models introduced in the previous section. Comparisons with the MP2 results indicate that the DFT may underestimate the barriers to proton transfer somewhat; however such benchmarking should ideally be extended to higher levels of theory in the future.

In the calculations presented below, all the geometry structures are therefore optimized by DFT at the B3LYP/6-31+g** level. Harmonic frequency calculations are performed for all stationary points to verify that they are genuine minima or transition states (TSs). Intrinsic reaction coordinate (IRC) calculations are carried out to elaborate the pathway connecting the TS to the reactant and product geometries. The pathways have been computed in mass-weighted internals with the step size set to $0.02 \text{ amu}^{-1} \text{ bohr}$.^{40,41} All calculations are performed with the Gaussian 03 package.⁴²

4. Energy Profiles and Structural Features of the Reaction Pathways

We begin with some discussion of the essential features of the single-proton-transfer model. Single-proton transfer has been extensively studied for models of different biomolecular systems (e.g., refs 43 and 44), and many of the typical features are apparent in the present case also. The energy profile obtained for proton transfer from the HBDI chromophore donor to the formate ion acceptor is given in Figure 3. Also shown are the optimized structures for the neutral cluster, the transition state, and the anionic cluster. Frequency calculations at the saddle-point geometry yield a single pure imaginary frequency at $298.5i \text{ cm}^{-1}$, corresponding to a stretching mode of the proton between the donor and the acceptor oxygen atoms. It is apparent from Figure 3 that proton transfer for the single-proton model is a low-barrier, fast process. This proves also to be the case for the two- and three-proton-transfer models (Figures 6 and 8 below). Although it is not shown on the plots, in each case the harmonic zero-point vibrational channel at the barrier lies below the harmonic zero-point level of the neutral cluster, implying that the neutral cluster may not be vibrationally bound and the hydrogen thence delocalized for these cluster models. This issue, while not central to the mechanistic considerations of this paper, is discussed critically further in section 5 below.

The chromophore backbone structure at the TS is close to the structure of the anionic form, with clear evidence from the changes in bond lengths of the onset of conjugation between the two resonance structures of the anionic HBDI. For example, the C–O bond of phenol reduces from 1.318 \AA in the neutral cluster to 1.297 \AA at the transition state and finally to 1.290 \AA in the anionic cluster. The key structural parameters associated with the neutral, TS, and anionic optimized geometries are given in Table 2 for all three of the models, and Figures 4a–c show the atomic labeling notation that is used in Table 2.

The distance between the donor and the acceptor oxygen atoms is 2.408 \AA at the transition state, while it is 2.469 \AA at the neutral cluster optimized geometry and 2.437 \AA at the anionic cluster optimized geometry. This reveals the well-known phenomenon that the donor and acceptor groups “breathe” inward as the proton is moving between them^{43,44} to help stabilize the charge—at least, insofar as the MEP is concerned.

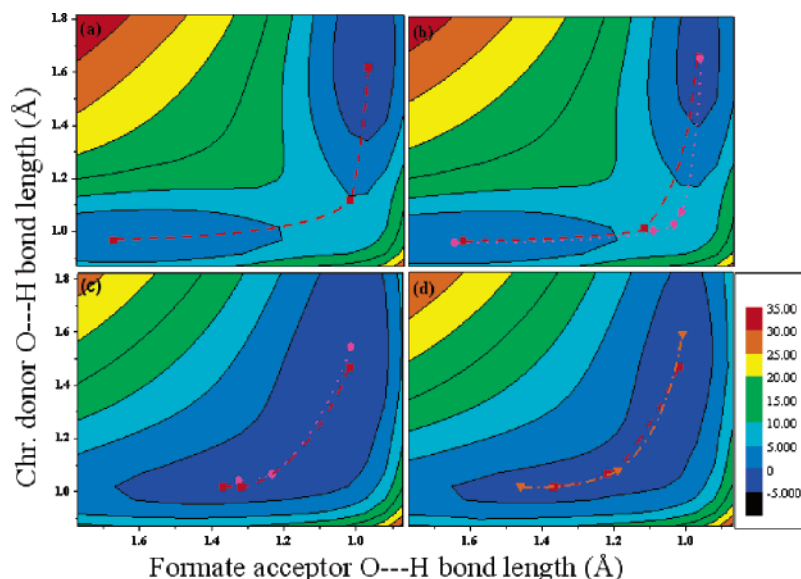


Figure 2. Two-dimensional relaxed potential energy surfaces for the two-proton-transfer model at different levels of theory and basis set. Contour colors are defined in the legends (in kcal/mol), in each case relative to energy of the starting neutral configuration: (a) HF/6-31g*; (b) HF/6-31+g**/HF/6-31g*; (c) B3LYP/6-31+g**/HF/6-31g*; (d) MP2/6-31+g**/HF/6-31g*. Squares with the dashed line represent the approximate MEP estimated directly from analysis of the contours on the 2-D PES. Circles with the dotted line and triangles with the dash-dotted line show the configurations mapped out by the true MEPs in parts b, c, and d with HF/6-31+g**, B3LYP/6-31+g** and MP2/6-31g*, respectively.

TABLE 1: Relative Energetics (in kcal/mol) for the Two-Proton-Transfer Model^a

	neutral form	transition state	anionic form
HF/6-31g*	0	5.7	-4.0
HF/6-31+g**	0	5.7	-2.0
	(0)	(6.7)	(-1.0)
B3LYP/6-31+g**	0	0.03	-2.8
	(0)	(0.03)	(-2.9)
MP2/6-31g*	(0)	(0.9)	(-4.5)
MP2/6-31+g**	0	0.2	-1.5

^a The upper line in each cell shows the estimates obtained directly from the 2-D relaxed potential energy surfaces of Figure 2. In parentheses are the barriers obtained from full MEP calculations (with barriers verified as true saddle points) where available.

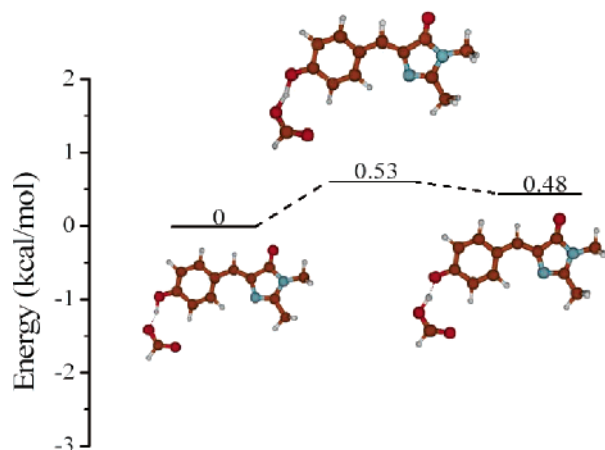


Figure 3. Optimized structures and energy profile for the one-proton-transfer model.

This characteristic correlation between donor-acceptor separation and displacement of the proton is revealed clearly by a plot of the normalized displacement of the proton in comparison with the normalized separation of the donor and acceptor oxygen atoms.²⁶ This comparative plot is shown for the single-proton-transfer case in Figure 5. In this figure the “relative displacement”, D_{OH} , at a given point i along the reaction path (or MEP)

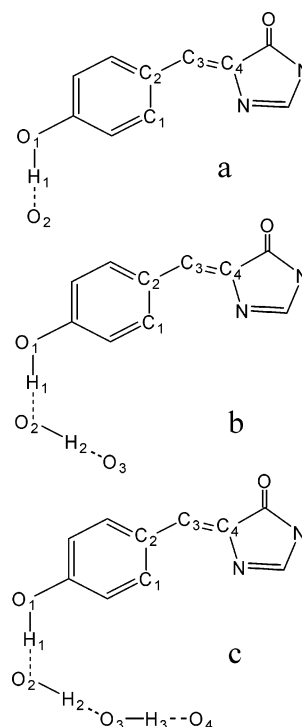


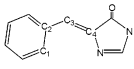
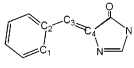
Figure 4. Atom labeling scheme used for describing the structural parameters in Table 2: (a) single-proton-transfer model; (b) two-proton chain transfer model; (c) three-proton chain transfer model.

is defined as the change in OH bond length from the previous grid point, normalized against the average of such displacements along the whole reaction pathway

$$D_{OH} = \frac{b_{i+1} - b_i}{\frac{1}{n} \sum_{i=1}^n (b_{i+1} - b_i)} \quad (1)$$

The “relative separation”, D_{OO} , is defined as the separation between the donor and the acceptor oxygen atoms, normalized

TABLE 2: Geometrical Parameters of the Models from B3LYP/6-31+g Calculations**

	single-proton model			two-proton model			three-proton model		
	N	TS	A	N	TS	A	N	TS	A
C-O of phenol	1.318	1.297	1.290	1.327	1.322	1.285	1.349	1.322	1.283
C ₂ -C ₃	1.431	1.425	1.423	1.436	1.435	1.423	1.447	1.435	1.423
C ₃ =C ₄	1.373	1.378	1.379	1.369	1.370	1.379	1.360	1.370	1.379
C=O	1.235	1.237	1.238	1.233	1.233	1.237	1.230	1.233	1.237
O ₁ -H ₁	1.074	1.257	1.351	1.042	1.066	1.473	0.996	1.071	1.516
H ₁ -O ₂	1.410	1.171	1.106	1.479	1.416	1.046	1.708	1.404	1.032
O ₂ -H ₂				1.118	1.187	1.559	1.010	1.209	1.621
H ₂ -O ₃				1.325	1.233	1.020	1.596	1.204	1.004
O ₃ -H ₃							1.057	1.397	1.582
H ₃ -O ₄							1.443	1.075	1.013
O ₁ ...O ₂	2.469	2.408	2.437	2.520	2.482	2.517	2.702	2.474	2.547
O ₂ ...O ₃				2.575	2.420	2.442	2.605	2.412	2.623
O ₃ ...O ₄							2.499	2.472	2.592
C-O-H	117.3	124.6	127.5	113.3	113.8	122.3	111.1	115.0	124.5
 dihedral C ₁ -C ₂ -C ₃ -C ₄	0.009	0.013	0.002	0.028	0.008	0.323	2.546	0.006	0.115
 dihedral C ₂ -C ₃ -C ₄ -N	0.004	0.161	0.001	0.021	0.069	0.027	0.199	0.005	0.093

against the average value of this separation over the whole reaction path

$$D_{\text{OO}} = \frac{d_i}{\frac{1}{n} \sum_{i=1}^n d_i} \quad (2)$$

Figure 5, as with the analogous Figures 7 and 9 below, constitutes an analysis of the specific changes in system configuration at the grid points along the computed MEP. For the purposes of the mechanistic observations to be elaborated below, one could consider the upper panels alone since they show the ordering of the movement of the protons. However, since the correlations of the proton movements with the breathing movements of the respective donor and acceptor oxygen pairs are also quite interesting and further support the arguments about ordering, we have displayed the two panels stacked together in each of the figures.

It is clear that the separation between the donor and the acceptor oxygen atoms is minimized at essentially the same point where the proton displacement is maximized and that this in fact coincides closely with the location of the potential barrier for the single-proton-transfer model, indicated in Figure 4 by the vertical gray line. We will return to this same type of plot for the two- and three-proton models below, with quite striking outcomes.

Figure 6 shows the energy profile and optimized stationary point geometries for the two-proton chain transfer model. One

observes first again that this is a low-barrier, fast proton-transfer process for the cluster model. The reaction path (MEP) is also traced out on the two-dimensional relaxed PES of Figure 2c (the dotted line, with diamonds indicating the stationary points). At the B3LYP/6-31+g** level of theory one transition state structure is obtained with an imaginary frequency of 264.7i cm⁻¹, the corresponding normal mode for which is categorically

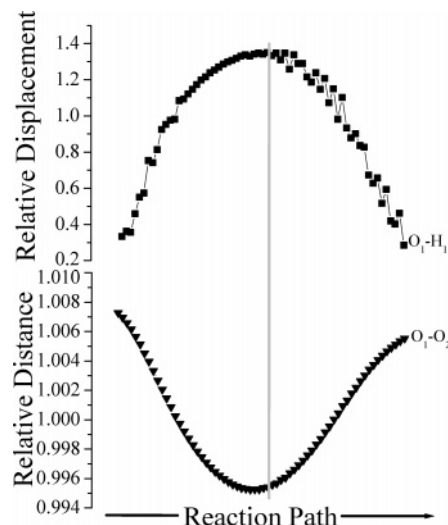


Figure 5. O-H bond relative displacement and the relative donor-acceptor distance for the one-proton-transfer model, determined from analysis of geometries along the minimum energy pathway. The position of the transition state is indicated by the vertical gray line.

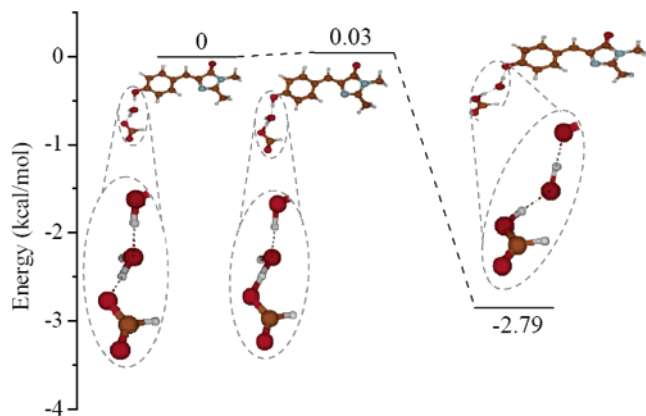


Figure 6. Optimized structures and energy profile for the two-proton chain transfer model.

an O–H stretching mode between the bridging water and the formate ion acceptor. Hence, as is also clearly apparent from examination of the structures in Figure 6, the motions at the barrier involve movement of a proton off the bridging water toward the formate acceptor, while the proton on the chromophore essentially has not moved. The specific values for the structural parameters are provided in Table 2.

Given that the TS involves movement of a proton off the bridging water toward the accepting formate group, while the proton on the chromophore has barely moved, it is not surprising that the backbone HBDI chromophore structure at the transition state is much closer to the neutral form. This is in distinct contrast to the single-proton-transfer model and can be seen very clearly from examination of the parameters in Table 2. For example, the C–O bond length on the phenol group of HBDI, which will ultimately shorten in the anionic structure, has barely changed at the TS for the two-proton chain transfer model—in marked contrast to the single-proton-transfer model. This observation in fact is the rationalization for the procedure utilized in preparing the benchmarking data of Figure 2, in which the internal coordinates of the chromophore were frozen at their neutral geometries for the purpose of generating the two-dimensional potential maps at different levels of theory and basis set, thereby speeding up the calculations significantly. (We note again, however, that no such constraints are involved for the full MEP/IRC calculations.)

Figure 7 shows the comparative plot of the relative displacements of the two mobile hydrogen atoms (H1 and H2) and the relative separations of the corresponding donor and acceptor pairs (O1–O2 and O2–O3, Figure 4b), obtained by analysis of the geometries along the reaction path as in eqs 1 and 2. Intriguingly, despite the fact that there is only one barrier and there are no stable intermediates along the reaction path, Figure 7 reveals a very clear signature of sequential movement of the two mobile protons. The first proton to move is from the bridging water to the formate acceptor, corresponding precisely with the “breathing” motion of the O2–O3 donor–acceptor pair of oxygens. This is the stage that corresponds to the low barrier, as indicated by the vertical gray line. After passing over the barrier, H1 moves finally from the chromophore across onto the bridging water in precise correspondence with the breathing movement of the O1–O2 donor–acceptor pair.

Finally, we consider the results of the three-proton chain transfer model. The energy profile in Figure 8 again reveals a low-barrier, fast proton transfer for this cluster model. There is a single transition state along the reaction path (MEP) that links the neutral and anionic forms of the cluster, with an imaginary frequency of $512.9i \text{ cm}^{-1}$. This corresponds categorically to an

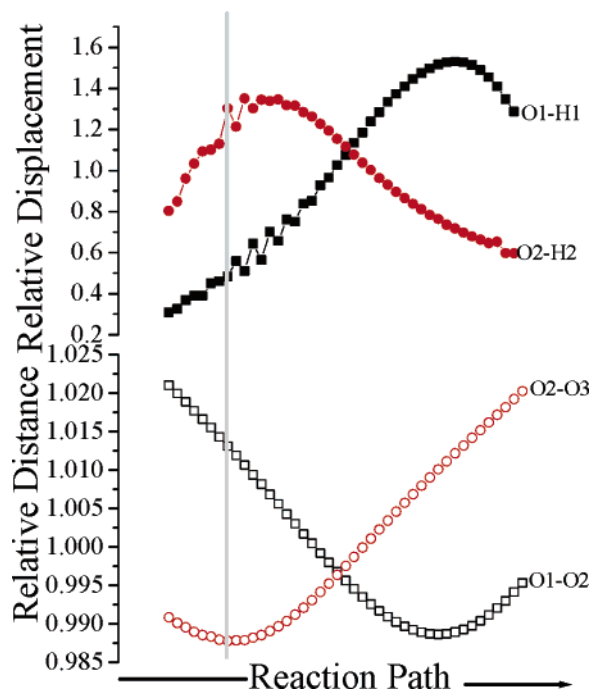


Figure 7. Relative displacement of mobile protons H1 and H2 and corresponding relative donor–acceptor distances for the two-proton chain transfer model, determined from analysis of geometries along the minimum energy pathway. The position of the transition state is indicated by the vertical gray line.

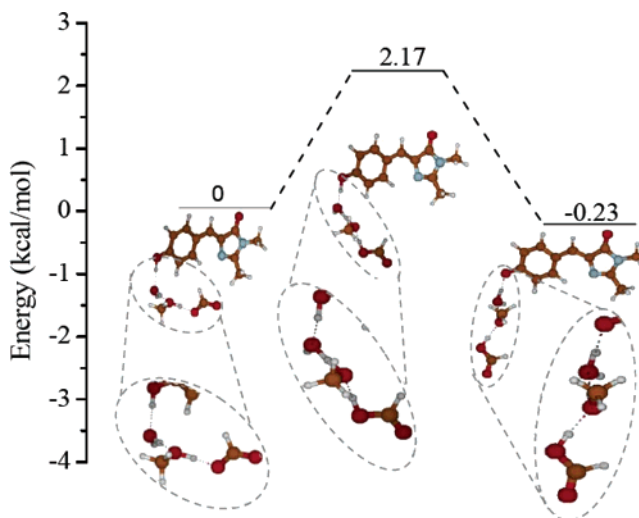


Figure 8. Optimized structures and energy profile for the three-proton chain transfer model.

O–H stretching mode between bridging water and methanol moieties. The structures in Figure 8 reveal the following features of the TS: (i) The third mobile proton H3 (Figure 4c) has already moved from the bridging methanol to the formate acceptor group. (ii) Proton H2 is in the process of moving across from the water bridge to the methanol (or, at this point along the reaction path, perhaps better termed methoxide) bridge. (iii) Proton H1 has barely moved and still resides essentially on the chromophore. As in the two-proton chain transfer model, the fact that the proton H1 has barely moved off the chromophore at the TS explains why the backbone structure of the HBDI chromophore at the transition state (Table 2) is closer to that of the neutral form.

Figure 9 shows the relative displacements of protons H1, H2, and H3 and the relative separations of the corresponding O1–O2, O2–O3, and O3–O4 donor–acceptor pairs, determined

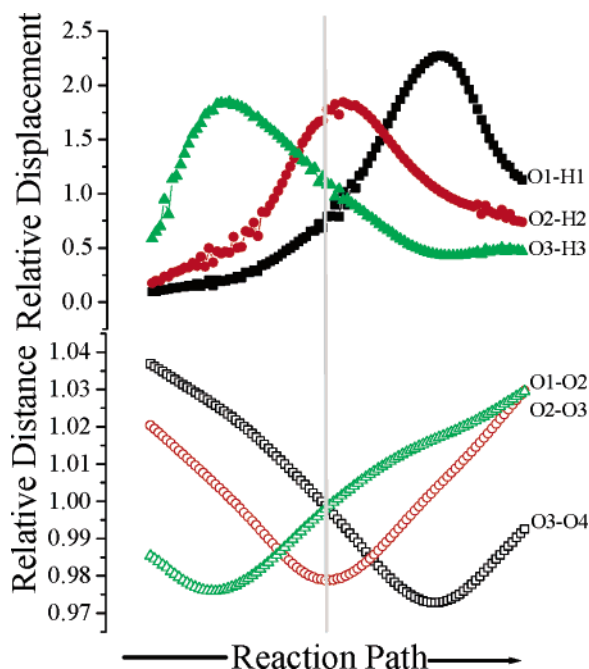


Figure 9. Relative displacement of mobile protons H1, H2, and H3 with corresponding relative donor–acceptor distances for the three-proton chain transfer model, determined from analysis of geometries along the minimum energy pathway. The position of the transition state is indicated by the vertical gray line.

from analysis of the reaction pathway geometries. There are two remarkable features of this plot. First, and for the purposes of this paper most importantly, is the fact that even though there is only a single barrier along the reaction pathway (Figure 8), there is again a clear signature of sequential movement of the protons in the chain transfer. Consistent with the results for the two-proton model, the last proton in the chain moves first to the formate acceptor group. For the three-proton model, this is followed by the middle proton in the chain moving between the first and the second bridge moieties, and finally the first proton moves off the chromophore to the water bridge, yielding the anionic chromophore. Ensuing from this first observation of sequential motion of the protons along the reaction coordinate, the second remarkable feature of Figure 9 is the fact that the correlation between proton movement and the “breathing” of the donor–acceptor pair, which is well established for single-proton transfers (e.g., refs 43 and 44), remains quite clearly an operative feature in the case of multiproton chain transfer as manifested in the present models.

5. Discussion

As mentioned in the Introduction, a common mechanistic theme in the study of proton chain transfer reactions is to establish whether the mechanism is stepwise or concerted. Notionally, a stepwise mechanism would involve sequential transfer of protons via one or more kinetically stable intermediates, while a concerted mechanism would involve simultaneous motion of all protons in a single kinetic step, characterized by a single barrier along the reaction coordinate.²⁶ The results of the previous section show that for the present cluster models, motivated by the chromophore and its immediate surroundings in GFP, the proton chain transfer occurs via a single barrier along the reaction pathway and in this sense would be regarded as “concerted”. This conclusion is in accord with the recent investigation of some different cluster models (also motivated by GFP) by Zhang et al.³³ However, while the term “concerted”

describes the kinetic situation correctly, it provides only a limited reflection of the nature of the motions along the reaction coordinate. Figures 7 and 9 provide unequivocal evidence of sequential movement of the protons in the chain, starting with the last proton moving onto the acceptor group and ending with the first proton moving off the chromophore. Hence, even within a concerted kinetic picture there are definite signatures of sequential movement of protons in the chain. The analysis represented in Figures 7 and 9 also provides insight into which O–H bond length coordinates play a dominant role in the reaction coordinate in different parts of the reaction path.

In all three of the models explored above, we see low barriers that would imply very fast proton transfer and a certain degree of delocalization in the hydrogen bonds. Although we have not shown the zero-point energies in Figures 3, 6, and 8, in each case the harmonic zero-point vibrational channel at the transition state lies beneath the harmonic zero-point energy level of the neutral cluster, similar to observations by Zhang et al.³³ and also by others in the context of single-proton transfer in low-barrier hydrogen bonds.⁴³ It is worthy of note, however, that the barrier to the reverse proton transfer (i.e., from the anionic form to the neutral form) in the ground state within GFP has been estimated experimentally to be somewhat higher than that calculated from our three-step model in Figure 8, on the order of 5–6 kcal mol^{−1}.⁴⁵ Additionally, the absolute time scale for reprotonation of the anionic chromophore on the ground-state potential energy surface, ca. 400 ps, has been uncovered recently by the use of ultrafast multipulse control spectroscopy.⁴⁶ While it is likely as inferred in Table 1 above that the DFT calculations somewhat underestimate the barriers involved, it is also true that subtle environmental effects within the protein not captured in the present cluster models will likely change the energetics and relative enthalpies of neutral and anionic states somewhat. We comment further on the possible limitations of cluster models such as those explored herein below.

In their cluster models, Zhang et al.³³ include a moiety to mimic the histidine residue His148 and stress its role in the proton-transfer process. It is certainly true that the His148 residue will play a significant role in solvating the negative charge on the phenolate oxygen of the anionic chromophore. The gas-phase energy profile of Zhang et al. (Figure 3 in ref 33) is therefore significantly more exothermic (ca. 3 kcal) than that shown above in Figure 8. However, we note that at the transition state of the three-proton chain transfer the proton H1 has barely moved off the chromophore. Hence, the solvating effect of the His148 residue is most likely to influence primarily the final enthalpy of the anionic state. Its solvating effect on the transition state, where the excess charge resides largely further along the chain, is likely to be less significant. This is a fundamentally different situation to single-proton transfer, where neighboring groups adjacent to the donor can have a much more direct and substantive effect in solvating the donor’s developing negative charge at the transition state. Thus, while the gas-phase energy profile of Zhang et al. is significantly more exothermic than ours, the barrier height that they obtain is quite similar (ca. 1.2 kcal higher) to that in Figure 8. Other minor differences in the two cluster models prevent a more detailed comparison.

Interestingly, analysis of the Mulliken charges on the donor, bridging, and acceptor oxygens (O1–O4 in Figure 4c) at the geometries along the IRC of the three-proton chain transfer model reveals the gradual transfer of charge from the Glu222 residue along the proton wire to the chromophore as well as provides another signature for the sequential motion of protons

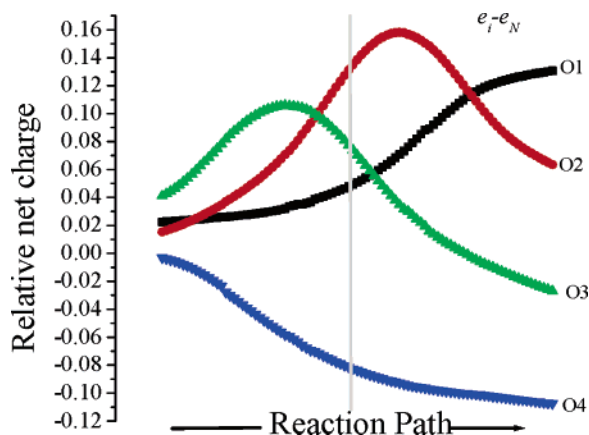


Figure 10. Difference between the Mulliken charge e_i at a given point i along the reaction coordinate and the charge e_N at the optimized geometry for the neutral structure, for each of the aforementioned oxygens.

along the reaction coordinate. In Figure 10 we plot the difference between the Mulliken charge e_i at a given point i along the reaction coordinate and the charge e_N at the optimized geometry for the neutral structure, for each of the aforementioned oxygens. As the third proton in the chain moves initially from the methanol bridge to the formate acceptor group, we see the net charge on O4 begin to decline while the charge on O3 rises. Then, as the middle proton in the chain moves between the water bridge and the methanol bridge, the charge on O3 starts to decline and the charge on O2 rises. Finally, as the first proton moves off the chromophore onto the bridging water, the charge on O2 drops and the charge on O1 rises.

Despite the role of the His148 terminal group in solvating the anionic structure of the chromophore, we have not chosen to pursue this aspect of the cluster model further in the present work. There are in principle a number of groups that one could further include to consider stabilization of various parts of the chromophore and its hydrogen-bonded network. It would seem that inclusion of His148 alone actually skews the endothermicity too far in favor of the anionic structure in comparison with the wild-type protein, since under ambient conditions the neutral form in the ground state is favored by a population ratio of 6:1 over the structurally relaxed anionic form.¹ Aside from the enthalpic issues discussed above, it should also be borne in mind that entropically related quantities (zero-point energies, partition functions) for such cluster models need also to be treated with caution, for the simple reason that the degree of flexibility (impacting on the vibrational manifold) is sensitive to the specific cluster model and may not be faithfully representative of the actual mechanical constraints on the key moieties within the protein. For these reasons, we do not give more detailed consideration to such entropic and enthalpic properties of the models that we have explored in this work.

Notwithstanding the cautionary comments of the previous paragraph, we are strongly encouraged by the remarkably consistent mechanistic picture coming out of the two-proton and three-proton chain transfer models studied above. Even though the enthalpies and barrier heights are significantly different for the two cluster models as shown in Figures 6 and 8 (as of course are the harmonic zero-point effects), the picture of sequential motion of the protons, starting with the final proton in the chain jumping to the acceptor group and ending with the first proton moving off the chromophore, is strikingly consistent for both models as shown by Figures 7 and 9. Thus, we believe that the principle mechanistic conclusions of this work may have broader

significance for proton chain transfer mechanisms in biomolecular systems.

It is interesting to note that the mechanistic picture arising from our detailed quantum chemical calculations on the cluster models bears some similarities, but also some differences, to the conclusions derived by Lill and Helms²³ in their molecular dynamics simulations of the $A \leftrightarrow I$ proton shuttle in GFP. Reference 23 implicitly adopts the ansatz of a stepwise hopping mechanism (in contrast to the concerted picture arising from the present work as well as that of Zhang et al.³³), wherein stochastic jumps are made based on approximate quantum transmission probabilities. Their method predicted that the first proton hop in the $I \rightarrow A$ ground-state proton chain transfer would involve reprotonation of the chromophore from the bridging water. This is qualitatively consistent with the reaction path mechanism that we have elaborated from our models but of course in the reverse direction. Their modeling indicated, however, that this first hop is strongly rate limiting with the second and third protons “backing up” on a femtosecond time scale. Such a picture would suggest a conventional kinetic isotope effect associated with the movement of a single proton in the rate determining step. The recent experiments of Kennis et al.⁴⁶ indicated a kinetic isotope effect for the ground-state $I \rightarrow A$ transformation of approximately 12, which is consistent with the likelihood of a kinetically concerted proton chain transfer mechanism rather than a stepwise hopping mechanism with one rate determining step. The results of the present study are compatible in parts with both pictures, since we see a kinetically concerted process (a single barrier for the overall proton chain transfer) within which one can still discern the tendency for the protons to move sequentially in the same qualitative order as predicted by Lill and Helms.²³

Finally, some comment on the possible relevance of our conclusions to the excited-state proton transfer (ESPT) in GFP is relevant. In their recent work, Vendrell et al.²⁰ have carried out TD-DFT, CASSCF, and CASPT2 calculations for ESPT using a simple cluster model consisting of the HBDI chromophore as the donor and a water molecule as the acceptor. Analogous to the case of ESPT in phenols,²¹ they have found a ${}^1\pi\sigma^*$ excited state that intersects with the photoexcited ${}^1\pi\pi^*$ state as the phenolic O—H bond is stretched, suggesting that this may constitute an alternative volume-conserving pathway for radiationless deactivation of the GFP chromophore. While their conclusions are potentially very relevant for the interpretation of HBDI spectroscopy in water, there are a number of features about the proton chain transfer pathway in GFP that give cause for caution before extrapolating the same conclusion to the protein. First, as has also been pointed out by Zhang et al.³³ in relation to the work of Lill and Helms,²³ one notes that the barrier for pushing a proton from HBDI onto a neutral water molecule is very large (ca. 2–3 eV), and indeed the proton-transfer product (anionic chromophore and H_3O^+) is not stable at all unless the water is constrained to be sufficiently far away from the chromophore, due the charge separation that is created. This, of course, is a function of the relatively weak basicity of the water molecule. In this context, it is perhaps not surprising that the charge-transfer ${}^1\pi\sigma^*$ state (which creates a radical cluster corresponding effectively to hydrogen transfer) is competitive in terms of energetics. In the case of GFP, however, one has proton chain transfer to the negatively charged Glu222 residue. The presence of the untitrated Glu222 acceptor group at the end of the proton wire may have a profound effect on the energetics of this concerted proton-transfer process and most likely will impact substantially on the relative energetics of the

two excited electronic states investigated by Vendrell et al.²⁰ In the case of ground-state proton transfer as elaborated above, the effect is such that proton transfer from chromophore to water is not the first step along the reaction coordinate. Rather, transfer from the Ser205 bridge to the Glu222 acceptor is inferred as the first step by our cluster model calculations, followed by proton transfer from water to Ser205. Hence, for the three-proton chain transfer model, substantial negative charge has already built up on the water bridge before the proton starts to move off the chromophore (Figure 10). Whether such a mechanistic picture carries over to ESPT in GFP is a very complex and unresolved issue, particularly in light of the known increased acidity of the phenol moiety in the excited state. It should also be noted that our mechanistic conclusions are based on minimum energy pathway calculations, which tend to be relevant for thermally induced reactions dominated by the low-energy pathways. In this sense, again, the conclusions are therefore most appropriate with reference to the ground-state $I \rightarrow A$ part of the GFP proton shuttle, and inferences for the ESPT process must clearly be tentative only. Clearly, further exploratory calculations in this regard will be an important direction for future research, as flagged by Vendrell et al.²⁰

6. Conclusions

The green fluorescent protein is an extraordinarily versatile tool for noninvasive cellular imaging and because of its great utility has been studied intensively over the past 15 years. Critical to the photophysical function of this protein is the triple-proton chain transfer event, by which the neutral chromophore undergoes fast proton transfer to the protein matrix to yield the green fluorescent anionic chromophore. After the fluorescence, the reverse proton transfer on the ground electronic state potential energy surface reconstitutes the neutral chromophore. We have in this paper investigated the mechanism for ground-state proton chain transfer in GFP, using cluster models of varying complexity to represent the chromophore, bridging species and the Glu222 acceptor. Our investigation shows categorically, in agreement with the recent work of Zhang et al.,³³ that the proton-transfer process is concerted and fast, with a single potential barrier along the reaction coordinate and no stable intermediates. While it is possible that the protein matrix may impact upon the precise details of the potential profile along the reaction pathway, that the concerted mechanism is an intrinsic property of the chromophore and its immediate proton-transfer pathway in the absence of additional environmental effects is established by these two works. Furthermore, the picture of a kinetically concerted mechanism for the proton chain transfer on the ground-state potential energy surface is consistent with a large kinetic isotope effect as observed experimentally by Kennis et al.⁴⁶

The present work reveals additionally an intriguing mechanistic insight that despite the overall "concerted" nature of the potential profile the configurational evolution along the reaction coordinate involves *sequential* movement of the protons. For the neutral to anionic proton chain transfer, first to move is the last proton in the chain from the methanol bridge to the formate ion accepting group. This is followed by transfer of a proton from the water bridge to the methanol bridge and finally by transfer of the phenolic proton from the chromophore to the bridging water. In the reverse proton transfer on the ground-state surface from the anionic to the neutral structures, which occurs in the GFP absorption/fluorescence cycle, the ordering will be reversed and is consistent with that inferred by Lill and Helms.²³

Our mechanistic exploration also reveals a significant contrast between single-proton transfer and proton chain transfer in relation to neighboring group (NG) effects, wherein developing charge on the donor is solvated by a nearby residue (typified by the His148–chromophore interactions in the wild-type GFP). We find that such specific NG–chromophore interactions are likely to influence primarily the overall reaction enthalpy, with a lesser effect on the barrier height for proton transfer. This is because substantial negative charge develops on the donor only late along the reaction coordinate, post transition state. At the transition state, the negative charge still resides primarily on the bridging moieties; hence solvation effects from nearby residues are likely to be rather more complex.

Acknowledgment. We gratefully acknowledge generous grants of computing time at The University of Queensland (Computational Molecular Science cluster computing facility) and the Australian Partnership for Advanced Computing National Facility.

Supporting Information Available: Geometries (in Cartesian coordinates) and computed absolute energies of all the stationary points illustrated in Figures 3, 6, and 8 as well as the imaginary frequencies for the transition states. This material is available free of charge via the Internet at <http://pubs.acs.org>.

References and Notes

- (1) Tsien, R. Y. *Annu. Rev. Biochem.* **1998**, *67*, 509–544.
- (2) Chatteraj, M.; King, B. A.; Bublit, G. U.; Boxer, S. G. *Proc. Natl. Acad. Sci. U.S.A.* **1996**, *93*, 8362–8367.
- (3) Lossau, H.; Kummer, A.; Heinecke, R.; Pöllinger-Dammer, F.; Kompa, C.; Bleser, G.; Jonsson, T.; Silva, C. M.; Yang, M. M.; Youvan, D. C.; Micheal-Beyerle, M. E. *Chem. Phys.* **1996**, *213*, 1–16.
- (4) Creemers, T. M. H.; Lock, A. J.; Subramaniam, V.; Jovin, T. M.; Voelker, S. *Nat. Struct. Biol.* **1999**, *6*, 557–560.
- (5) Winkler, K.; Lindner, J.; Subramaniam, V.; Jovin, T. M.; Vöhringer, P. *Phys. Chem. Chem. Phys.* **2002**, *4*, 1072–1081.
- (6) Cubitt, A. B.; Heim, R.; Adams, S. R.; Boyd, A. E.; Gross, L. A.; Tsien, R. Y. *Trends Biochem. Sci.* **1995**, *20*, 448–455.
- (7) Prasher, D. C. *Trends Genet.* **1995**, *11*, 320–323.
- (8) Gerdes, H.-H.; Kaether, C. *FEBS Lett.* **1996**, *389*, 44–47.
- (9) He, X.; Bell, A. F.; Tonge, P. J. *J. Phys. Chem. B* **2002**, *106*, 6056–6066.
- (10) Niwa, H.; Inouye, S.; Hirano, T.; Matsuno, T.; Kojima, S.; Kubota, M.; Ohashi, M.; Tsuji, F. I. *Proc. Natl. Acad. Sci. U.S.A.* **1996**, *93*, 13617–13622.
- (11) Brejc, K.; Sixma, T. K.; Kitts, P. A.; Kain, S. R.; Tsien, R. Y.; Ormö, M.; Remington, J. *Proc. Natl. Acad. Sci. U.S.A.* **1997**, *94*, 2306–2311.
- (12) Warren, A.; Zimmer, M. *J. Mol. Graphics Modell.* **2001**, *19*, 297–303.
- (13) Zimmer, M. *Chem. Rev.* **2002**, *102*, 759–781.
- (14) Helms, V. *Curr. Opin. Struct. Biol.* **2002**, *12*, 169–175.
- (15) Chen, M. C.; Lambert, C. R.; Urigiti, J. D.; Zimmer, M. *Chem. Phys.* **2001**, *270*, 157–164.
- (16) Weber, W.; Helms, V.; McCammon, J. A.; Langhoff, P. W. *Proc. Natl. Acad. Sci. U.S.A.* **1999**, *96*, 6177–6182.
- (17) Toniolo, A.; Ben-Nun, M.; Martinez, T. J. *J. Phys. Chem. A* **2002**, *106*, 4679–4689.
- (18) Toniolo, A.; Granucci, G.; Martinez, T. J. *J. Phys. Chem. A* **2003**, *107*, 3822–3830.
- (19) Martin, M. E.; Negri, F.; Olivucci, M. *J. Am. Chem. Soc.* **2004**, *126*, 5452–5464.
- (20) Vendrell, O.; Gelabert, R.; Moreno, M.; Lluch, J. M. *Chem. Phys. Lett.* **2004**, *396*, 202–207.
- (21) Sobolewski, A. L.; Domcke, W. *J. Phys. Chem. A* **2001**, *105*, 9275–9283.
- (22) Laino, T.; Nifosi, R.; Tozzini, V. *Chem. Phys.* **2004**, *298*, 17–28.
- (23) Lill, M. A.; Helms, V. *Proc. Natl. Acad. Sci. U.S.A.* **2002**, *99*, 2778–2781.
- (24) Reuter, N.; Lin, H.; Thiel, W. *J. Phys. Chem. B* **2002**, *106*, 6310–6321.
- (25) Litvinenko, K. L.; Webber, N. M.; Meech, S. R. *Bull. Chem. Soc. Jpn.* **2002**, *75*, 1065–1070.
- (26) Isaev, A.; Scheiner, S. *J. Phys. Chem. B* **2001**, *105*, 6420–6426.

- (27) Lu, D.; Voth, G. A. *J. Am. Chem. Soc.* **1998**, *120*, 4006–4014.
- (28) Lill, M. A.; Hutter, M. C.; Helms, V. *J. Phys. Chem. A* **2000**, *104*, 8283–8289.
- (29) Lill, M. A.; Helms, V. *J. Chem. Phys.* **2001**, *114*, 1125–1132.
- (30) Lill, M. A.; Helms, V. *Proc. Natl. Acad. Sci. U.S.A.* **2002**, *99*, 2778–2781.
- (31) Cui, Q.; Karplus, M. *J. Phys. Chem. B* **2003**, *107*, 1071–1078.
- (32) Chen, H.; Li, S.; Jiang, Y. *J. Phys. Chem. A* **2003**, *107*, 4652–4660.
- (33) Zhang, R.; Nguyen, M. T.; Ceulemans, A. *Chem. Phys. Lett.* **2005**, *404*, 250–256.
- (34) Helms, V.; Winstead, C.; Langhoff, P. W. *J. Mol. Struct.* **2000**, *506*, 179–189.
- (35) Nielsen, S. B.; Lapierre, A.; Andersen, J. U.; Pedersen, U. V.; Tomita, S.; Andersen, L. H. *Phys. Rev. Lett.* **2001**, *87*, 228102.
- (36) Schellenberg, P.; Johnson, E.; Esposito, A. P.; Reid, P. J.; Parson, W. W. *J. Phys. Chem. B* **2001**, *105*, 5316–5322.
- (37) Litvinenko, K. L.; Webber, N. M.; Meech, S. R. *Chem. Phys. Lett.* **2001**, *346*, 47–53.
- (38) Mandal, D.; Tahara, T.; Webber, N. M.; Meech, S. R. *Chem. Phys. Lett.* **2002**, *358*, 495–501.
- (39) Wang, S.; Smith, S. *Chem. Phys.*, in press.
- (40) Gonzalez, C.; Schlegel, H. B. *J. Chem. Phys.* **1989**, *90*, 2154–2161.
- (41) Gonzalez, C.; Schlegel, H. B. *J. Phys. Chem.* **1990**, *94*, 5523–5527.
- (42) Frisch, M. J.; Trucks, G. W.; Schlegel, H. B.; Scuseria, G. E.; Robb, M. A.; Cheeseman, J. R.; Montgomery, J. A., Jr.; Vreven, T.; Kudin, K. N.; Burant, J. C.; Millam, J. M.; Iyengar, S. S.; Tomasi, J.; Barone, V.; Mennucci, B.; Cossi, M.; Scalmani, G.; Rega, N.; Petersson, G. A.; Nakatsuji, H.; Hada, M.; Ehara, M.; Toyota, K.; Fukuda, R.; Hasegawa, J.; Ishida, M.; Nakajima, T.; Honda, Y.; Kitao, O.; Nakai, H.; Klene, M.; Li, X.; Knox, J. E.; Hratchian, H. P.; Cross, J. B.; Bakken, V.; Adamo, C.; Jaramillo, J.; Gomperts, R.; Stratmann, R. E.; Yazyev, O.; Austin, A. J.; Cammi, R.; Pomelli, C.; Ochterski, J. W.; Ayala, P. Y.; Morokuma, K.; Voth, G. A.; Salvador, P.; Dannenberg, J. J.; Zakrzewski, V. G.; Dapprich, S.; Daniels, A. D.; Strain, M. C.; Farkas, O.; Malick, D. K.; Rabuck, A. D.; Raghavachari, K.; Foresman, J. B.; Ortiz, J. V.; Cui, Q.; Baboul, A. G.; Clifford, S.; Cioslowski, J.; Stefanov, B. B.; Liu, G.; Liashenko, A.; Piskorz, P.; Komaromi, I.; Martin, R. L.; Fox, D. J.; Keith, T.; Al-Laham, M. A.; Peng, C. Y.; Nanayakkara, A.; Challacombe, M.; Gill, P. M. W.; Johnson, B.; Chen, W.; Wong, M. W.; Gonzalez, C.; Pople, J. A. *Gaussian 03*, revision B.05; Gaussian, Inc.: Wallingford, CT, 2004.
- (43) Perrin, C. L.; Nielson, J. B. *Annu. Rev. Phys. Chem.* **1997**, *48*, 511–544.
- (44) Del Bene, J. E.; Jordan, M. J. T. *Int. Rev. Phys. Chem.* **1999**, *18*, 119–162.
- (45) Seebacher, C.; Deeg, F. W.; Bräuchle, C. *J. Phys. Chem. B* **1999**, *103*, 7728–7732.
- (46) Kennis, J. T. M.; Larsen, D. S.; van Stokkum, I. H. M.; Vengris, M.; van Thor, J. J. *Proc. Natl. Acad. Sci. U.S.A.* **2004**, *101*, 17988–17993.